



LAWRENCE  
LIVERMORE  
NATIONAL  
LABORATORY

# Direct Observations of Sigma Phase Growth and Dissolution in 2205 Duplex Stainless Steel

T.A. Palmer, J.W. Elmer, S.S. Babu, E.D. Specht

June 17, 2005

Trends in Welding Research  
Pine Mountain, GA, United States  
May 16, 2005 through May 20, 2005

## **Disclaimer**

---

This document was prepared as an account of work sponsored by an agency of the United States Government. Neither the United States Government nor the University of California nor any of their employees, makes any warranty, express or implied, or assumes any legal liability or responsibility for the accuracy, completeness, or usefulness of any information, apparatus, product, or process disclosed, or represents that its use would not infringe privately owned rights. Reference herein to any specific commercial product, process, or service by trade name, trademark, manufacturer, or otherwise, does not necessarily constitute or imply its endorsement, recommendation, or favoring by the United States Government or the University of California. The views and opinions of authors expressed herein do not necessarily state or reflect those of the United States Government or the University of California, and shall not be used for advertising or product endorsement purposes.

# Direct Observations of Sigma Phase Growth and Dissolution in 2205 Duplex Stainless Steel

**T.A. Palmer, J.W. Elmer**

*Lawrence Livermore National Laboratory, Livermore, CA, United States*

**S.S. Babu**

*Formerly, Oak Ridge National Laboratory, Oak Ridge, TN, United States  
Currently, Edison Welding Institute, Columbus, OH, United States*

**E.D. Specht**

*Oak Ridge National Laboratory, Oak Ridge, TN, United States*

## Abstract

The formation and growth of sigma ( $\sigma$ ) phase in a 2205 duplex stainless steel is monitored during an 850°C isothermal heat treatment using an in situ synchrotron x-ray diffraction technique. At this temperature,  $\sigma$  phase is first observed within approximately 40 seconds of the start of the isothermal heat treatment and grows rapidly over the course of the 3600 second heat treatment to a volume fraction of approximately 13%. A simultaneous increase in the austenite ( $\gamma$ ) volume fraction and a decrease in the ferrite ( $\delta$ ) volume fraction are observed. The  $\sigma$  phase formed at this temperature is rapidly dissolved within approximately 200 seconds when the temperature is increased to 1000°C. Accompanying this rapid dissolution of the  $\sigma$  phase, the  $\delta$  and  $\gamma$  volume fractions both approach the balanced (50/50) level observed in the as-received material.

## Introduction

When duplex stainless steels (DSS) are exposed to temperatures between approximately 600°C and 1000°C for sustained periods of time, several undesirable intermetallic phases, which include  $\sigma$ ,  $\chi$ ,  $\pi$ , can form.[1-2] These intermetallic phases negatively impact both the mechanical properties and the corrosion resistance of duplex stainless steels.[3-9] The sigma ( $\sigma$ ) phase is the most prominent of these intermetallic phases. It generally forms over a temperature range between 600°C and 1000°C, depending on the alloy being considered and the specific alloying elements included. [1-3] It is primarily composed of Fe, 29-34 wt.% Cr, 3-5 wt.% Ni, and 3-9 wt.% Mo. If Si and W are present in the alloy, they are also observed in the  $\sigma$  phase.[1]

Much of the existing research on  $\sigma$  phase formation and growth is based on results obtained using optical and electron microscopy based techniques on as-cast and welded material.[10-12] There are a number of shortcomings and disadvantages associated with this experimental methodology. In particular, these techniques provide only a snapshot of the phases present after the completion of an isothermal heat treatment, including the effects of both heating and cooling, which can not be factored

out of the final measurements. When using metallographic techniques, it is also difficult to discern between the different intermetallic phases when measuring the volume fractions of each phase present in the heat treated microstructure.

By using x-ray diffraction, especially high intensity synchrotron x-rays, transformations occurring during an isothermal heat treatment, heating, and cooling, can be monitored in real time. This technique has recently been applied to the study of phase transformations and residual stress relaxation in Ti-6Al-4V.[13,14] These types of in situ studies have a number of inherent advantages over more conventional optical metallographic techniques in the study of phase transformations. Whereas the identification of low volume fraction intermetallic phases with optical microscopy has some uncertainty, there is none when using the x-ray diffraction technique because each phase produces characteristic peaks. By analyzing these peaks, the volume fractions of each phase along with other changes in the characteristics of the phases which may be occurring during the transformation can be quantified.

In the work discussed here, a synchrotron based in situ x-ray diffraction technique is used to monitor the formation and growth of  $\sigma$  phase during an isothermal heat treatment at a temperature of 850°C. Additional experiments showing the dissolution of the  $\sigma$  phase at a temperature of 1000°C from a heat treated microstructure is also discussed. Along with the formation and growth of the  $\sigma$  phase, the formation and growth of austenite ( $\gamma$ ) and the dissolution of ferrite ( $\delta$ ) are also found to occur.[15-17]. These transformations are also monitored in real time. The combination of these observations provides a complete picture of the transformations occurring in this material at this temperature. Results from this work will provide a basis for more in-depth investigations of the transformation kinetics involved with  $\sigma$  phase formation and dissolution and the corresponding  $\delta/\gamma$  transformations

## Experimental

**Material Properties** Figure 1(a) shows the A typical microstructure for the as-received 10.8 cm diameter 2205 DSS forged

bar stock (22.43 Cr-4.88 Ni-3.13 Mo-1.40 Mn-0.023 C-0.18 N-0.004 S-0.005 O-0.0007H-0.67 Si-0.02 Al-0.03 B-0.08 Co-0.20 Cu-0.03 Nb-0.028 P-<0.005 Ti-0.05 V- Bal. Fe). This microstructure is revealed using an electrolytic KOH etch (25 gm KOH, 50 mL water) held at a voltage of 2V for approximately 15 sec.[10-11] The  $\gamma$  is the lightly etched phase and exists as elongated plates in a  $\delta$  matrix, which is the darkly etched phase. Quantitative metallography has been previously performed on this material and shows a  $\delta$ : $\gamma$  ratio of 54:46 in the as-received condition. The  $\sigma$  phase, which forms at the  $\delta$ / $\gamma$  boundaries in the wrought DSS material after aging, appears as the most darkly etched phase. A typical microstructure containing significant amounts of  $\sigma$  phase formed after a prolonged 850°C isothermal heat treatment is shown in Figure 1(b).

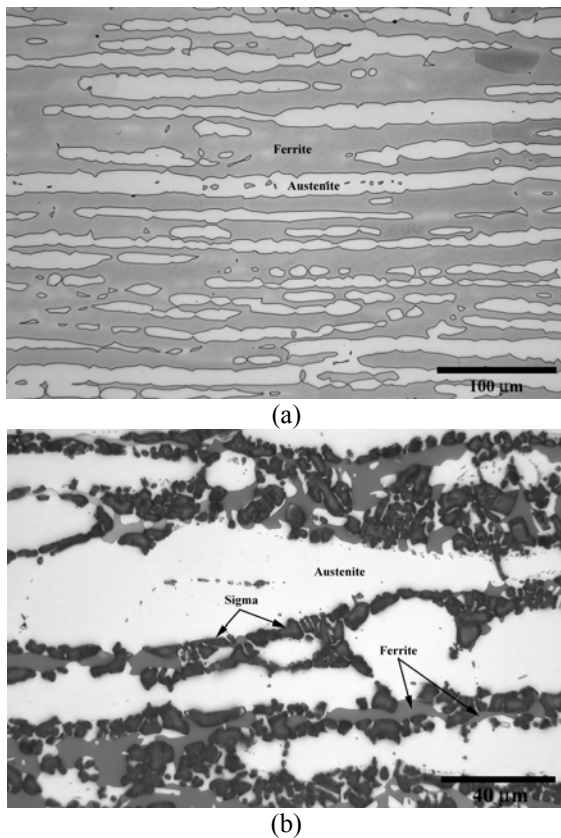


Figure 1(a&b): Optical micrographs of (a) a typical base metal microstructure and (b)  $\sigma$  phase in the 2205 DSS sample aged at 850°C for 36000 seconds.

An equilibrium phase diagram for this alloy has been calculated using ThermoCalc® and the TC Fe2000 database. Figure 2 shows the resulting phase diagram at temperatures between 600°C and 975°C, considering only  $\delta$ ,  $\gamma$ , and  $\sigma$  as stable. According to these calculations, the  $\delta$  phase displays a significant decrease in its volume fraction leading up to 650°C and disappears completely from approximately 665°C to 875°C. Over this temperature range, the  $\sigma$  phase decreases slightly, while the  $\gamma$  phase gradually increases. At 875°C, the  $\delta$  phase reappears and

begins growing, while the amount of  $\sigma$  phase decreases. The  $\sigma$  phase completely dissolves at a temperature of approximately 940°C, leaving  $\delta$  and  $\gamma$  with similar fractions. It needs to be noted, though, that these calculations are based on equilibrium conditions, whereas the microstructure in the 2205 DSS is formed by a high temperature heat treatment (1065°C) and quench and is metastable at room temperature.

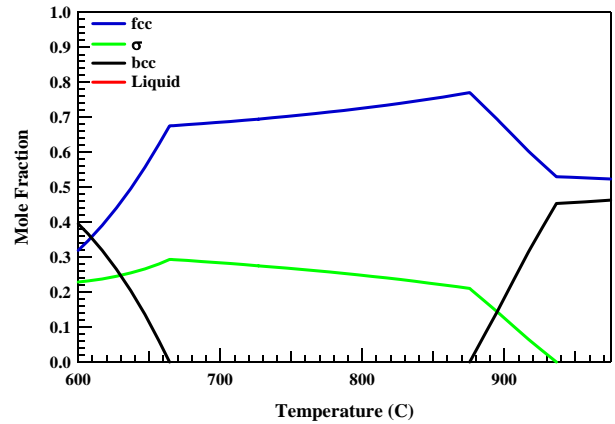


Figure 2: Calculated portion of the phase diagram between 600°C and 975°C for the 2205 DSS.

**X-Ray Diffraction Experiments** Direct resistance heating of the 100 mm long by 4.75mm wide by 2 mm thick 62 micron rms finish samples is used for rapid heating. Water cooled grips allow the sample to be rapidly cooled. The temperature of the sample was monitored and recorded using type-S (Pt/Pt-10%Rh) thermocouples spot welded on the back side of the sample directly below the x-ray impingement point. A Eurotherm 818 temperature controller, a Eurotherm 425A power thyristor, and a Trindl RT300 transformer were used to control the AC current passing through the sample so that pre-programmed thermal cycles could be followed in a controlled manner. The heating power supply is capable of producing 300 Amps at 6V and can heat the sample up to temperatures as high as 1400°C. The sample and heating and cooling stage assembly are placed inside a vacuum chamber in order to protect it from atmospheric contamination during the prolonged heating cycles. Prior to each experiment, the chamber is evacuated and maintained under vacuum during the entirety of each experimental run.

In-situ x-ray diffraction experiments are performed using the UNICAT beam line BM-33-C at the Advanced Photon Source (APS) at the Argonne National Laboratory. A beam energy of 30 keV from a ring current of 100mA is used. Prior to the beam coming in contact with the sample, it first passes through a water cooled Si (111) monochromator and is then focused and sized to dimensions of 1 mm wide by 0.25 mm high using a dynamically bent Si crystal and collimator slits. In these experiments, the x-ray beam impinges on the top surface of the sample at a 5° angle of incidence while the sample is being heated. The 528  $\mu$ m x-ray absorption length provides a penetra-

tion depth of at least 23  $\mu\text{m}$ , which can become larger at higher Bragg angles. A schematic diagram of the experimental setup is shown in Figure 3.

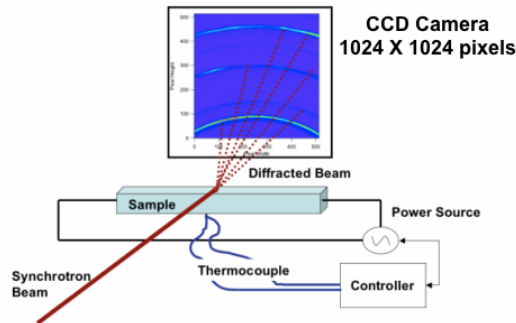


Figure 3: Schematic of the apparatus used in the synchrotron x-ray diffraction experiments.

The diffracted beams are collected using a Roper Scientific (A99k401, RS/Photometrics) CCD detector placed 330 mm behind the sample. This detector uses a 12.9  $\text{cm}^2$  array of 1024x1024 pixels spaced 60 microns apart to capture the diffraction patterns on a scintillating screen, which is connected to the CCD array using a fiber optic bundle. The detector read-out is accelerated by a 2x2 binning of the pixels. In these experiments, the detector integrates the x-ray data over a one second exposure and requires an additional two seconds to clear the data from the CCD detector and transfer it to the computer. Thus, it is possible to capture a complete diffraction pattern approximately every 3 seconds. Depending on the length of the experiment and the amount of data desired, this rest time can be varied. For example, a 10 second rest time is used in the long term 850°C isothermal heat treatment described below. A room temperature x-ray diffraction pattern of an as-received 2205 DSS sample is shown in Figure 4 for d spacings between approximately 1.1 to 2.4  $\text{\AA}$ .

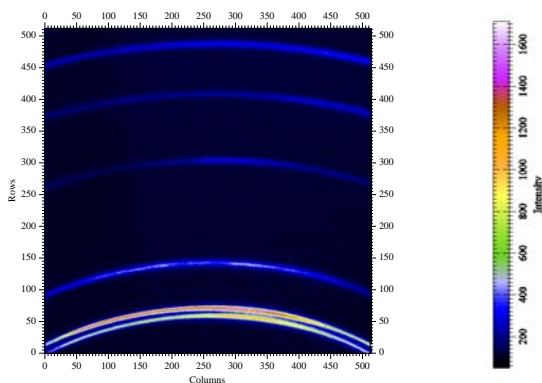


Figure 4: Plot showing the partial Debye circles obtained using the CCD detector for the base metal 2205 DSS.

To calibrate the x-ray detector, the room temperature lattice parameters of the base metal are first measured using a conventional  $\text{Cu K}\alpha$  x-ray diffraction system. A room temperature pattern, as shown in Figure 4, is then collected. Five points are selected along each of the Debye arcs. The sample-detector distance, the position of the center of the arcs on the detector, and the magnitude and orientation of the detector tilt are varied to minimize the difference between the d spacing as calculated from the detector patterns and that calculated from the lattice parameters. The Debye arcs are then integrated into a one dimensional plot showing diffracted beam intensity versus d spacing using Fit-2D software [18]. This software integrates the diffracted beam intensity for each arc, providing the data used to create the diffraction patterns used in the following analysis.

Characteristics of the individual peaks are then determined using a macro developed for Igor Pro, Version 5.0. With this macro, the time and temperature at which each diffraction pattern is obtained are linked with the corresponding diffraction data. In order to take into account any variations in the intensity of the synchrotron beam, the intensities of the peaks in each diffraction pattern are normalized with respect to the maximum peak intensity measured in that pattern. A typical diffraction pattern showing the presence of  $\sigma$  phase along with the  $\delta$  and  $\gamma$  phases in a 2205 DSS sample undergoing an 850°C isothermal heat treatment is shown in Figure 5. Each peak is identified with the appropriate phase and corresponding Miller indices.

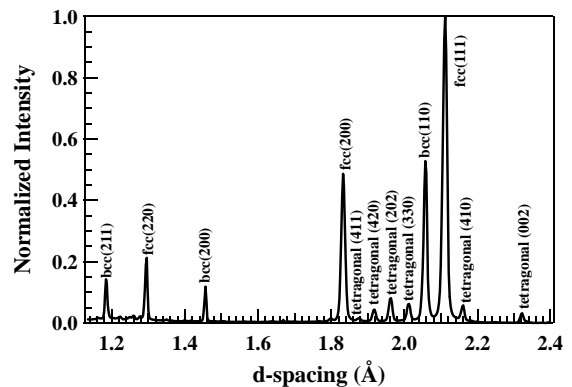


Figure 5: Typical diffraction pattern showing  $\delta$ ,  $\gamma$ , and  $\sigma$  phases detected during an 850°C isothermal heat treatment.

After the normalization of the diffraction pattern, the position, width (FWHM), and integrated intensity of each peak are measured. Using the integrated intensity measurements for each of these peaks, the volume fractions of the three primary phases ( $\delta$ ,  $\gamma$ , and  $\sigma$ ) are measured by summing the integrated intensities for the peaks from each phase and dividing this value by the sum of the integrated intensity values for all of the peaks observed in each diffraction pattern.

## Results and Discussion

**Formation and Growth of  $\sigma$  Phase** Using this in situ x-ray diffraction technique, the formation and growth of the  $\sigma$  phase are monitored as a function of time during an isothermal heat treatment at a temperature of 850°C and a time of 36000 seconds. Figure 6 displays a pseudo-color plot of the peak intensities measured at each time over the initial 3600 seconds of this isothermal heat treatment. Only this portion of the isothermal heat treatment is shown because there is little obvious change in the peak intensities at the longer times. Soon after the start of the isothermal heat treatment, at a time of approximately 40 seconds, tetragonal  $\sigma$  phase peaks appear. These peaks are present over the remainder of the isothermal heat treatment and increase in intensity as the time increases.

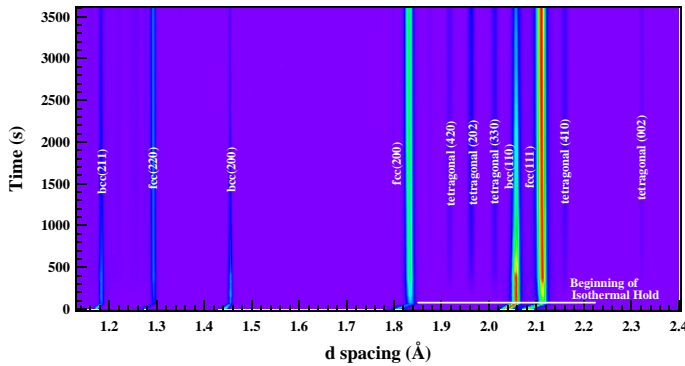


Figure 6: Pseudo-color plot of peak intensities taken over the first 3600 seconds of the 850°C isothermal heat treatment of the 2205 DSS.

At the same time, changes in the intensities of the  $\delta$  and  $\gamma$  peaks are taking place. In general, the  $\delta$  peaks decrease in intensity and the  $\gamma$  peaks increase in intensity with increasing time. Based on the plot in Figure 6, it appears that these changes in the  $\delta$  and  $\gamma$  peak intensities correspond with the appearance and increasing intensity of the tetragonal or  $\sigma$  phase peaks. These changes are especially evident in the fcc(111) and bcc(110) peaks, which appear to swap intensity values at a time of approximately 300 seconds.

A closer look at the measured intensities of the fcc(111) and bcc(110) peaks is given in Figure 7. Shortly after the beginning of the isothermal heat treatment, the intensity of the fcc (111) peak rapidly increases, while that for the bcc(110) peak remains mostly constant. At a time of approximately 300 seconds, the intensity of the fcc(111) peak reaches a constant value, while that for the bcc(110) peak begins a rapid decrease which continues for the remainder of the isothermal heat treatment. These peak intensity measurements are then converted into the volume fractions of each phase present at each discrete time over the course of the isothermal heat treatment.

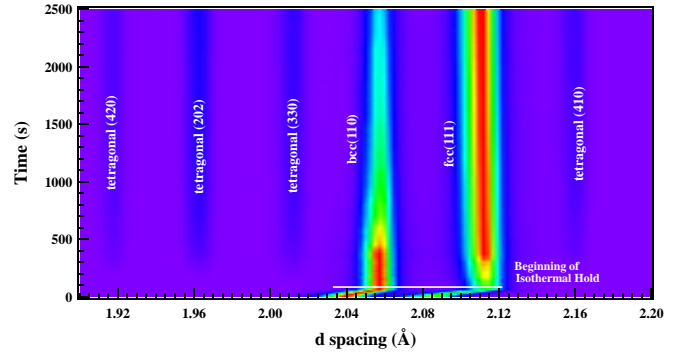


Figure 7: Pseudo-color plot highlighting the changes in peak intensities for the fcc(111) and bcc(110) peaks in the early stages of the 850°C isothermal heat treatment.

A plot of these measurements taken during the 850°C isothermal hold is shown in Figure 8. As the isothermal heat treatment begins, the  $\gamma$  volume fraction increases while the  $\delta$  volume fraction decreases, as predicted by the changes in integrated intensity. Within this same time frame,  $\sigma$  phase first appears and rapidly grows through the first 5000 seconds of the heat treatment. After this time, the measured volume fraction of the  $\sigma$  phase remains rather constant over the remaining portion of the isothermal heat treatment. The same is true for both the  $\gamma$  and  $\delta$  volume fractions, indicating that the microstructure is reaching some level of stability.

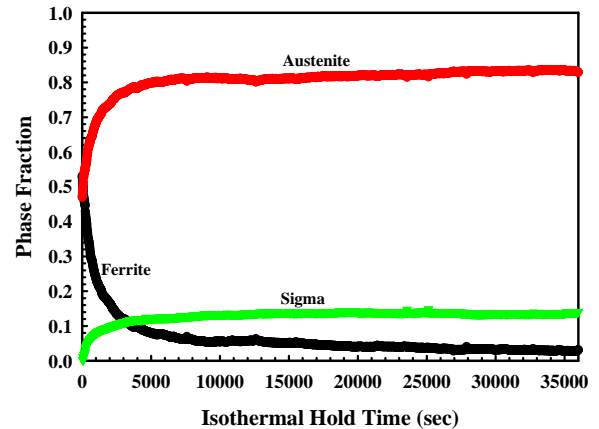


Figure 8: Plot showing the  $\gamma$ ,  $\delta$ , and  $\sigma$  volume fractions measured over the course of the 850°C isothermal heat treatment.

The biggest changes in the measured volume fractions of the three phases occur in the early stages of the isothermal heat treatment. It is clear that the  $\delta$  and  $\gamma$  volume fractions are changing from the beginning. A summary of the volume fractions measured during the 850°C isothermal heat treatment is given in Table 1. Over the first 5000 seconds, there are significant changes in the measured volume fractions of all three phases, especially the  $\sigma$  phase, which displays its most rapid growth rate, rising to a volume fraction of 0.121. After that point, the  $\sigma$

volume fraction rises only an additional 0.018 over the remainder of the isothermal heat treatment.

Table 1: Summary of  $\delta$ ,  $\gamma$ , and  $\sigma$  volume fractions at selected times during the 850°C isothermal heat treatment

	Ferrite	Austenite	Sigma
As-received	0.548	0.452	---
Beginning (t = 0 sec)	0.530	0.470	---
t = 42 seconds	0.504	0.494	0.002
t = 5000 seconds	0.080	0.799	0.121
t = 10000 seconds	0.054	0.812	0.134
End (t = 36141 seconds)	0.038	0.823	0.139

Significant changes are also occurring in the  $\delta$  and  $\gamma$  phases. For example, the  $\delta$  volume fraction falls from a value of 0.530 at the beginning of the isothermal hold to a value of 0.080 after 5000 seconds, equating to a decrease of approximately 85%. Over this same time frame, the  $\gamma$  volume fraction increases from 0.470 to 0.799, equating to an approximately 70% increase. By the end of the isothermal heat treatment, the  $\delta$  volume fraction has fallen to a value of 0.038 and the  $\gamma$  volume fraction has risen to a value of 0.823. These two values do not differ much from those measured at a time of 10000 seconds, indicating that the transformation rate significantly slows at times greater than 5000 seconds.

These results indicate that  $\delta$  is transforming into both  $\gamma$  and  $\sigma$  ( $\delta \rightarrow \gamma + \sigma$ ) at a temperature of 850°C. Since the  $\sigma$  phase grows at the expense of  $\delta$ , a decrease in the  $\delta$  volume fraction is expected. However, the  $\gamma$  volume fraction is increasing at the same time, indicating that the  $\delta$  phase is also decomposing into  $\gamma$  at this temperature. These observations are generally supported by the thermodynamic calculations shown in Figure 2.

The experimental results shown above, though, indicate that some  $\delta$  continues to exist in the microstructure and is expected to remain since the rate of transformation is approaching zero. A closer examination of Figure 2 shows that  $\delta$  should reappear in the microstructure at a temperature of 875°C. This difference of only 25°C may fall within the uncertainty of these calculations. An additional factor in this discrepancy may also involve the metastable nature of the  $\delta$  in the starting microstructure.

**Dissolution of  $\sigma$  Phase** With the real-time detection capabilities of this technique, the dissolution of the  $\sigma$  phase can also be monitored. In order to directly monitor the  $\sigma$  phase dissolution, a two stage heat treatment is used. In the first stage, the sample is held at a temperature of 850°C for a period of 3600 seconds in order to form the  $\sigma$  phase in the 2205 DSS microstructure. After the  $\sigma$  phase forms, the temperature is rapidly increased to 1000°C and held until the  $\sigma$  phase disappears.

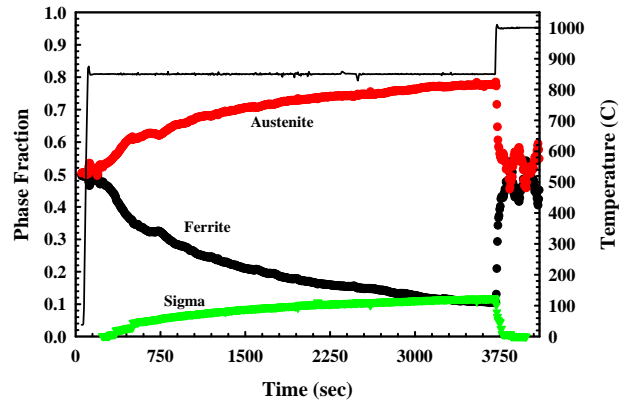


Figure 9: Plot showing changes in  $\delta$ ,  $\gamma$ , and  $\sigma$  volume fractions over the course of the 850°C to 1000°C heat treatment.

During the initial stage of the heat treatment, the changes in the  $\delta$ ,  $\gamma$ , and  $\sigma$  volume fractions closely resemble those observed previously. At the end of this isothermal heat treatment, the  $\sigma$  phase volume fraction reaches a level of approximately 0.13. The  $\delta$  and  $\gamma$  volume fractions at this same time are 0.105 and 0.779, respectively. These results are in line with those observed in the previous 850°C isothermal heat treatment.

The rapid dissolution of the  $\sigma$  phase is evident. With the increase in temperature to 1000°C, the  $\sigma$  phase, which is measured at a volume fraction of 0.13, disappears within 200 seconds. In comparison, an 850°C isothermal heat treatment of 3600 seconds is required to produce this amount of  $\sigma$  phase. This difference in transformation rates can, in part, be attributed to the higher temperature, which leads to both the destabilization of sigma phase as well as an increase in the diffusion kinetics.

In addition to the  $\sigma$  phase dissolution, changes in the  $\delta$  and  $\gamma$  volume fractions are also evident as the temperature is increased to 1000°C. As the  $\sigma$  phase dissolves, the  $\delta$  volume fraction rapidly increases. At the same time, the  $\gamma$  volume fraction decreases to a level of approximately 0.50, closely matching that of the  $\delta$  volume fraction. These changes in the  $\delta$  and  $\gamma$  volume fractions are predicted by the thermodynamic calculations in Figure 2 and further supported by the heat treatment (1065°C) performed on the as-received material to produce the balanced  $\delta/\gamma$  microstructure shown in Figure 1(a).

## Summary and Conclusions

A synchrotron based in situ x-ray diffraction technique has been used to monitor the formation, growth, and dissolution of  $\sigma$  phase in a 2205 DSS. During an 850°C isothermal heat treatment, the formation and growth of  $\sigma$  phase, along with  $\delta$  dissolution and  $\gamma$  growth, are directly monitored. In these real-time measurements,  $\sigma$  phase is first observed approximately 40 seconds after the start of this isothermal heat treatment. The rate of  $\sigma$  phase growth is most rapid over the initial 5000 seconds be-

fore slowing over the remainder of the isothermal heat treatment.

The dissolution of  $\sigma$  phase from a microstructure initially containing a  $\sigma$  volume fraction of approximately 0.13 is also monitored. Unlike the formation of the  $\sigma$  phase, its dissolution occurs rapidly, with the  $\sigma$  phase completely disappearing after only 200 seconds at a temperature of 1000°C, which is only 60°C above the predicted thermodynamic stability limit. The recovery of  $\delta$  and the decomposition of the newly formed  $\gamma$  phase are also monitored in real time along with the changes in the  $\sigma$  phase. These phases have recovered to nearly a 50/50 phase balance by the time that the  $\sigma$  phase completely dissolves.

These real-time observations of the changes in the  $\delta$ ,  $\gamma$ , and  $\sigma$  volume fractions also provide a basis for further study of the kinetics of these various transformations. Future work will use this experimental technique to construct TTT diagrams for  $\sigma$  phase formation and to calculate the transformation kinetics for the  $\delta \rightarrow \sigma$ ,  $\sigma \rightarrow \delta$ , and  $\delta \rightarrow \gamma$  transformations over this temperature range under isothermal conditions.

### Acknowledgements

The LLNL portion of this work was performed under the auspices of the U. S. Department of Energy, Lawrence Livermore National Laboratory, under Contract No. W-7405-ENG-48. The ORNL portion of this work was sponsored by the U.S. Department of Energy Division of Materials Sciences and Engineering under contract No. DE-AC05-00OR22725 with UT-Battelle, LLC. The UNICAT facility at the Advanced Photon Source (APS) is supported by the U.S. DOE under Award No. DEFG02-91ER45439, through the Frederick Seitz Materials Research Laboratory at the University of Illinois at Urbana-Champaign, the Oak Ridge National Laboratory (U.S. DOE contract DE-AC05-00OR22725 with UT-Battelle LLC), the National Institute of Standards and Technology (U.S. Department of Commerce) and UOP LLC. The APS is supported by the U.S. DOE, Basic Energy Sciences, Office of Science under contract No. W-31-109-ENG-38. The authors express gratitude to Bob Vallier of LLNL for performing optical metallography.

### References

1. L. Karlsson, *Intermetallic Phase Precipitation in Duplex Stainless Steels and Weld Metals: Metallurgy, Influence on Properties, Welding and Testing Aspects*, WRC Bulletin, 438 (1999)
2. J.-O. Nilsson, *Super Duplex Stainless Steels*, Mater. Sci. Technol., 8, 685-700 (1992).
3. L. Karlsson, L. Ryen, and S. Pak, *Precipitation of Intermetallic Phases in 22% Cr Duplex Stainless Steel Welds*, Weld. J., 74(1), 28s-40s (1995)
4. T.H. Chen, K.L. Weng, and J.R. Yang, *The Effect of High-Temperature Exposure on the Microstructural Stability and Toughness Property in a 2205 Duplex Stainless Steel*, Mater. Sci. Engin. A, A338, 259-70 (2002)
5. J.-O. Nilsson, P. Kangas, T. Karlsson, and A. Wilson, *Mechanical Properties, Microstructural Stability and Kinetics of  $\sigma$ -Phase Formation in 29Cr-6Ni-2Mo-0.38N Superduplex Stainless Steel*, Metall.Mater. Trans A, 31A, 35-45 (2000)
6. Y.S. Ahn, M. Kim, and B.H. Jeong, *Effect of Aging Treatments and Microstructural Evolution on Corrosion Resistance of Tungsten Substituted 2205 Duplex Stainless Steel*, Mater. Sci. Technol., 18, 383-8 (2002)
7. Y.S. Ahn and J.P. Kang, *Effect of Aging Treatments on Microstructure and Impact Properties of Tungsten Substituted 2205 Duplex Stainless Steel*, Mater. Sci. Technol., 16, 382-8 (2000)
8. J.-O. Nilsson and A. Wilson, *Influence of Isothermal Phase Transformations on Toughness and Pitting Corrosion of Super Duplex Stainless Steel SAF 2507*, Mater. Sci. Technol., 9, 545-54 (1993)
9. J. Li, T. Wu, and Y. Riquier,  *$\sigma$  Phase Precipitation and its Effect on the Mechanical Properties of a Super Duplex Stainless Steel*, Mater. Sci. Engin., A174, 149-56 (1994).
10. E. Johnson, Y.-J. Kim, L.S. Chumbley, and B. Gleeson, *Initial Phase Transformation Diagram Determination for the CD3MN Cast Duplex Stainless Steel*, Scripta Mater., 50, 1351-54 (2004)
11. Y.-J. Kim, L.S. Chumbley, and B. Gleeson, *Determination of Isothermal Transformation Diagrams for Sigma-Phase Formation in Cast Duplex Stainless Steels CD3MN and CD3MWCuN*, Metall. Mater. Trans. A, 35A, 3377-86 (2004)
12. J.-O. Nilsson, T. Huhtala, P. Jonsson, L. Karlsson, and A. Wilson, *Structural Stability of Super Duplex Stainless Steel Weld Metals and Its Dependence on Tungsten and Copper*, Metall. Mater. Trans. A, 27A, 2196-2208 (1996)
13. J.W. Elmer, T.A. Palmer, S.S. Babu, and E.D. Specht, *In-Situ Observations of Lattice Expansion and Transformation Rates of  $\alpha$  and  $\beta$  Phases in Ti-6Al-4V*, Materials Science and Engineering A, 391(1-2), 104-13 (2004)
14. J.W. Elmer, T.A. Palmer, S.S. Babu, and E.D. Specht, *Low Temperature Relaxation of Residual Stress in Ti-6Al-4V*, Scripta Mater., 52(10), 1051-6 (2005)
15. A. Gregori and J.-O. Nilsson, *Decomposition of Ferrite in Commercial Superduplex Stainless Steel Weld Metals; Microstructural Transformations above 700°C*, Metall. Mater. Trans. A, 33A, 1009-18 (2002)
16. C.H. Shek, G.J. Shen, J.K.L. Lai, and B.J. Duggan, *Early Stages of Decomposition of Ferrite in Duplex Stainless Steel*, Mater. Sci. Technol., 10, 306-11 (1994)
17. A.J. Ramirez, J.C. Lippold, and S.D. Brandi, *The Relationship between Chromium Nitride and Secondary Austenite Precipitation in Duplex Stainless Steels*, Metall. Mater. Trans. A, 34A, 1575-97 (2003)
18. A.P. Hammersley, *FIT2D V9.129 Reference Manual, V3.1*, ESRF Internal Report, ESRF98HA01T, 1998.